magnetochemistry

MDPI

Article

Viscous Effects on Nonlinear Double Tearing Mode and Plasmoid Formation in Adjacent Harris Sheets

Nisar Ahmad [1,†], Ping Zhu [2,3,*], Chao Shen [1,*], Ahmad Ali [4] and Shiyong Zeng [5]

[1] College of Science, Harbin Institute of Technology (Shenzhen), Shenzhen 518055, China; nisar@mail.ustc.edu.cn
[2] International Joint Research Laboratory of Magnetic Confinement Fusion and Plasma Physics, State Key Laboratory of Advanced Electromagnetic Engineering and Technology, School of Electrical and Electronic Engineering, Huazhong University of Science and Technology, Wuhan 430074, China
[3] Department of Engineering Physics, University of Wisconsin-Madison, Madison, WI 53706, USA
[4] Pakistan Tokamak Plasma Research Institute, Islamabad 3329, Pakistan
[5] Department of Plasma Physics and Fusion Engineering, University of Science and Technology of China, Hefei 230026, China
* Correspondence: zhup@hust.edu.cn (P.Z.); shenchao@hit.edu.cn (C.S.)
† Formerly at University of Science and Technology of China.

Abstract: In this paper, we study the effects of viscosity on the evolution of the double tearing mode (DTM) in a pair of adjacent Harris sheets based on the resistive MHD model in the NIMROD code. Similar to the tearing mode in the conventional single Harris sheet, a transition is observed in the generation of both normal and monster plasmoids at Prandtl number $P_r = 1$. In the $P_r < 1$ regime of the DTM, normal plasmoids (small plasmoids) are generated along with monster plasmoid, whereas in the single tearing mode (STM) cases, such a generation is not observed. When P_r is above the critical value, the generation of monster plasmoid is halted. Correspondingly, in the $P_r < 1$ regime, a quadrupolar flow advects along the poloidal direction, but in the $P_r > 1$ regime this flow advection is inhibited.

Keywords: double tearing mode; viscosity; reconnection; plasmoids; Prandtl number

Citation: Ahmad, N.; Zhu, P.; Shen, C.; Ali, A.; Zeng, S. Viscous Effects on Nonlinear Double Tearing Mode and Plasmoid Formation in Adjacent Harris Sheets. *Magnetochemistry* **2023**, *9*, 205. https://doi.org/10.3390/magnetochemistry9090205

Academic Editor: Roberto Zivieri

Received: 14 June 2023
Revised: 5 August 2023
Accepted: 18 August 2023
Published: 24 August 2023

1. Introduction

In recent years, magnetic reconnection and associated mechanisms regarding double tearing modes (DTM) have remained hot topics in the domain of space and fusion plasmas [1–4]. Different studies have reported the possible occurrence of double/multiple current sheets in space plasma [5–7]. One of the prominent examples to trigger double/multiple tearing modes [8–10] is the Earth's bow shock [11] . Reversed magnetic shear (RMS) is commonly formed in the modern setup of tokamak functioning [12], which can produce double tearing modes on two neighbouring rational surfaces having similar safety factors and the subsequent off-axis sawtooth oscillation/disruptions [13–17]. The magnetic reconfiguration caused by DTM has been extensively studied [13,14,18,19], which is among the most significant aspects of DTM's nonlinear evolution.

Many cases of multiple current sheet systems have been frequently examined during the observation of laboratory and space plasmas. A notable illustration of this phenomenon is found in tokamak discharges featuring central reversed magnetic shear [20,21]. Consequently, this configuration becomes a viable candidate for the uninterrupted functioning of a fusion reactor. However, it is notable that this specific setup may also lead to the initiation of a DTM [15,22–24], resulting in rapid magnetic reconnection and subsequent degradation of plasma confinement [17,25,26]. One crucial aspect of DTM's nonlinear evolution that has garnered extensive attention [13,14,18,19,27] is the alteration of magnetic configurations. It is widely known that when two resonant surfaces approach each other closely, the straggly-ordered islands found at distinct rational surfaces undergo enlargement and triangular deformation. This, in turn, leads to the generation of intense current density near the island's X-point, exciting subsequent intensive flow and fast reconnection. Many experts have studied the resistive, shear flow, large guiding field, and current sheet spacing effects on the nonlinear evolution of DTMs [28–32]. Through the nonlinear growth of a DTM, thin and lengthy current sheets can appear due to the island's interaction and detachment, instigating secondary/tertiary islands [29,33,34], displaying the variety and complicacy of physics hidden in the large magnetic Prandtl number P_r regime.

Usually, when the elongated current sheet's aspect ratio reaches a significant value, this narrow current sheet leads to the formation of plasmoids [34–38]. Plasmoids are distinct, coherent, and self-contained magnetic structures that can form in a plasma. Plasmoids typically have a toroidal or quasi-toroidal shape and are often interrelated with the magnetic reconnection events [39]. The formation of plasmoids often occurs in regions of intense magnetic fields and high plasma pressure [40–43]. In recent studies [33,44], multiple plasmoid formations were observed in the absence of viscosity in a simulation of multiple current sheet systems with high Lundquist number parameters. However, there has been limited research regarding the viscosity effects on the nonlinear evolution of DTMs. Minor electromagnetic perturbations may generate viscosity in tokamak plasmas [45]. As a class of the dissipation-producing effect, viscosity may also drive tearing mode instability, that can be from one of the plasma disruption causes [46–49]. The viscous tearing modes are one potential physical mechanism which produce rapid saw-tooth disruptions reported in experiments [50]. In slab-configuration plasmas, the linear features of DTMs owing to the viscosity have also been stated [51].

In this study, we employ the visco-resistive magnetohydrodynamic (MHD) model within the NIMROD code [52] to extensively investigate the nonlinear development of the double tearing mode. Our focus is on examining the impact of viscosity on the generation and evolution of plasmoids. Normal plasmoids (small plasmoids) [34] along with monster plasmoids appear in the $P_r < 1$ regime, whereas in the $P_r > 1$ regime, only monster plasmoids appear. The plasmoid dynamics in our simulations are compared with previous studies [53,54].

We present our numerical simulation details in Section 2. Our linear and nonlinear results are discussed in Sections 3 and 4, respectively. In Section 5, a summary of this paper is presented.

2. Model Equations

Our results are described by resistive MHD equations, which are implemented in the NIMROD code [52]. The visco-resistive MHD model (1)–(4) equations used in our study (presented below) are all non-dimensional.

$$\frac{\partial \rho}{\partial t} + \nabla \cdot (\rho \mathbf{v}) = 0 \tag{1}$$

$$\rho\left(\frac{\partial}{\partial t} + \mathbf{v}\cdot\nabla\right)\mathbf{v} = \mathbf{J}\times\mathbf{B} - \nabla p + \rho\nu\nabla^2\mathbf{v} \tag{2}$$

$$\frac{N}{\gamma - 1}\left(\frac{\partial}{\partial t} + \mathbf{v}\cdot\nabla\right)\mathbf{T} = -\frac{p}{2}\nabla\cdot\mathbf{v} \tag{3}$$

$$\frac{\partial \mathbf{B}}{\partial t} = \nabla\times(\mathbf{v}\times\mathbf{B} - \eta\mathbf{J}) = \nabla\times(\mathbf{v}\times\mathbf{B} - \eta\nabla\times\mathbf{B}) \tag{4}$$

where $\mathbf{B}, \mathbf{J}, N, \gamma, \mathbf{v}, p, \rho, \nu$ and η are the magnetic field, current density, number density, specific heat ratio, velocity, pressure, plasma mass density, viscosity, and resistivity, respectively. The Boltzmann constant (k) has been incorporated into the temperature ($\mathbf{T}$). The particle mass density ρ) and number density (N) are linked through the mass per ion. Additionally, the total temperature and pressure establish the ideal gas relation, $p = 2NT$, while taking into account rapid thermal equilibration and quasi-neutrality conditions between electrons and ions. The initial equilibrium profiles for $B_{0z}(x)$, $J_{0y}(x)$ and pressure are given below.

$$B_{0z}(x) = 1 - \tanh\left(\frac{x+x_0}{a}\right) + \tanh\left(\frac{x-x_0}{a}\right) \tag{5}$$

$$J_{0y}(x) = \frac{1}{a}\mathrm{sech}^2\left(\frac{x-x_0}{a}\right) - \frac{1}{a}\mathrm{sech}^2\left(\frac{x+x_0}{a}\right) \tag{6}$$

$$p_0(x) = T_0 + 0.5\left(1 - \tanh\left(\frac{x+x_0}{a}\right) + \tanh\left(\frac{x-x_0}{a}\right)\right)^2 \tag{7}$$

where the Cartesian coordinates (x, y, z) are adopted. The equilibrium profiles of $B_{0z}(x)$, $J_{0y}(x)$ and $p_0(x)$ at different resonance surfaces are plotted in Figure 1.

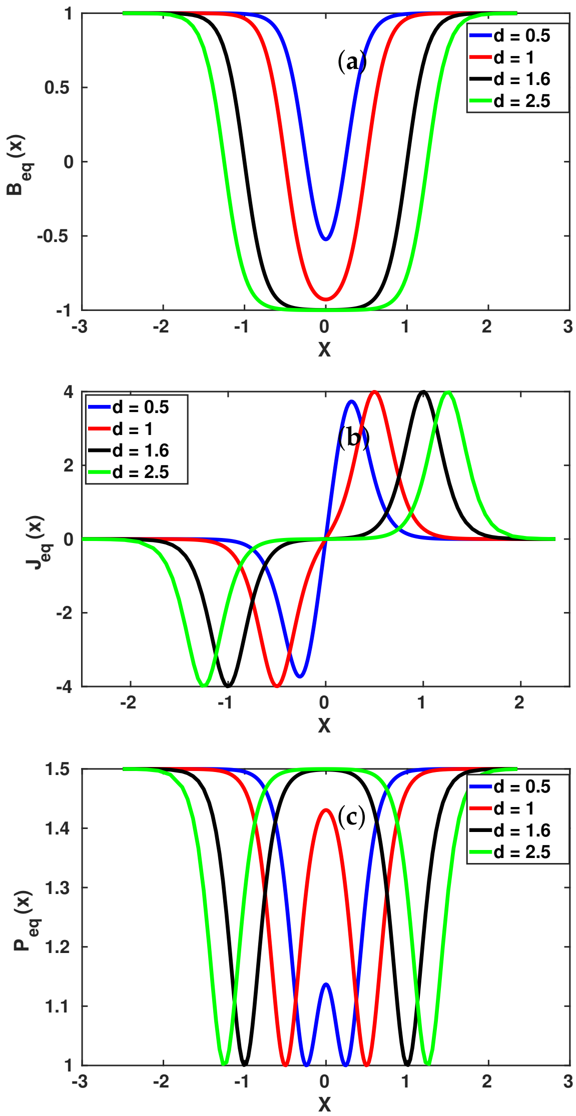

Figure 1. (**a**) Double Harris sheet equilibrium magnetic field, (**b**) current density and (**c**) pressure profiles at different distances between the rational surfaces.

Here, a controls the width of the profile (throughout this manuscript we have fixed the value of $a = 0.25$), T_0 is the constant equilibrium temperature, we also assume a uniform mass density ρ. The magnetic flux function is subjected to an initial perturbation, and its dynamic starting is initiated with an amplitude of 10^{-3} for the initial perturbation. To normalize the magnetic field, B_0 is used which is the field magnitude at $x \to \pm\infty$. The spatial normalization unit $x_0 = d/2$ represents half of the distance between the two adjacent current sheets. The mass density is normalized by ρ_0 at the center of the current sheets. To normalize time, pressure, and velocity $t_0 = \tau_{A0} = x_0/u_0 = x_0/u_{A0}$, $p_0 = B_0^2/\mu_0$, and $u_0 = u_{A0} = B_0/\sqrt{\mu_0\rho_0}$ are used, respectively. In the above simulation model, the adiabatic index is $\gamma = 5/3$ and the value of heat flux is assumed to be zero. In the above non-dimensional Equations (1-4), both the viscosity ν and the resistivity η are the normalised non-dimensional parameters, with $\nu = \frac{P_r}{S}$, and $S^{-1} = \eta$, where $S = \tau_R/\tau_{A0}$ represents the Lundquist number, $\tau_R = \mu_0 x_0^2/\eta_D$, here, η_D shows the un-normalized non-dimensional resistivity, and $P_r = \mu_0\nu_D/\eta_D$ represents the magnetic Prandtl number, ν_D is the un-normalized non-dimensional viscosity, having $\nu = \nu_D\tau_{A0}/x_0^2$.

To solve the above resistive MHD equations, a rectangular domain is employed with the form $[-L_x, L_x]\times[-L_y, L_y]$, with ranges $(-2.5, 2.5) \times (-5, 5)$, respectively. Here, we define the wave number as $L_y = 2\pi m/k$, where k represents the mode wave number in y direction, and m being the mode number. All boundary conditions along the y direction are periodic, whereas along the x direction all perturbations vanish.

3. Linear DTM Evolution

To understand the nonlinear behaviour of the DTM, we first examine a specific linear scenario. Linear mode structures of magnetic field, velocity and pressure are illustrated in Figure 2. Quadropolar flow cells can be observed in the velocity contours plots, which significantly influence magnetic reconnection [55]. When the rational surfaces are widely separated, these quadrupolar flow cells are partially advected along the current sheet. Understanding the role of these flow cells is crucial for the generation of plasmoids during the nonlinear dynamics of the DTM. Moreover, in the vicinity of the current sheet, the quadrupolar flow might either generate or annihilate.

In Figure 3a, the growth rate is drawn against η for different distances between the adjacent current sheets. In this study, kinetic energy is analyzed to determine the linear growth rate of the DTM. In this regime, this energy evolves exponentially: $E_K \sim e^{\gamma t}$. By using $\gamma = \partial_t(\ln E_K)$, γ can be obtained. For a fixed distance between the current sheets, a good agreement with existing theory is found at small value of η. However, for large values of η, it is observed that our results deviate from the existing theory [24]. From Figure 3a, we can also conclude that for a highly unstable system the power of η remains near to 0.33 which matches the scaling law for small distances between adjacent current sheets [24]. In Figure 3b, for different d within the range [0.5, 3], the parameter α (where α is $\gamma_{lin} = \eta^{\alpha}$) is plotted against distances between the current sheets. The transition between the scaling $\alpha = 3/5$ for large d and $\alpha = 1/3$ for small d is clearly observed in previous studies [56]. Our results do not match with the previous results because in their case the simulations were performed in cylindrical geometry whereas in our case we used Cartesian geometry. Additionally, the coupling of the flow eigen-function with the rational surfaces could be another reason. Due to this coupling, the mode represents the resistive kink mode. Furthermore, even in situations where the rational surfaces are distant from one another ($d = 1.6$), the tearing scaling with $\alpha = 3/5$ cannot be found due to the coupling. For small d, both effects, i.e., close rational surfaces and strongly coupled flows, might be the reason for the decreasing dependency with the resistivity ($\alpha \to 0.3$). This regime is well documented in [1,57].

It is found in Figure 4a that as the viscosity increases, the growth rate quickly slows down. The reduction in linear growth rates due to viscous dissipation is evident when viscosity is increased, as it counteracts resistive destabilization. Additionally, for a fixed value of distance between those rational surfaces, the growth rate exhibits a shift at $P_r = 1$. In the $P_r < 1$ regime, the impact of viscosity is insignificant whereas within the $P_r > 1$ regime, the growth rate decreases sharply. The viscous scaling for our simulations at $d = 0.5, 1$ and 2.5 are $\gamma \sim \nu^{-0.27}$, $\gamma \sim \nu^{-0.22}$ and $\gamma \sim \nu^{-0.25}$, respectively. These scaling results are very close to the theoretical scaling results [51,58]. From Figure 4b, for a fixed

Prandtl number, the growth rate decreases by increasing the distances between the current sheets or vice versa. It is observed that for $d < 0.5$, for a fixed Prandtl number, the growth rate remains constant but for $d > 0.5$, the growth rate decreases quickly.

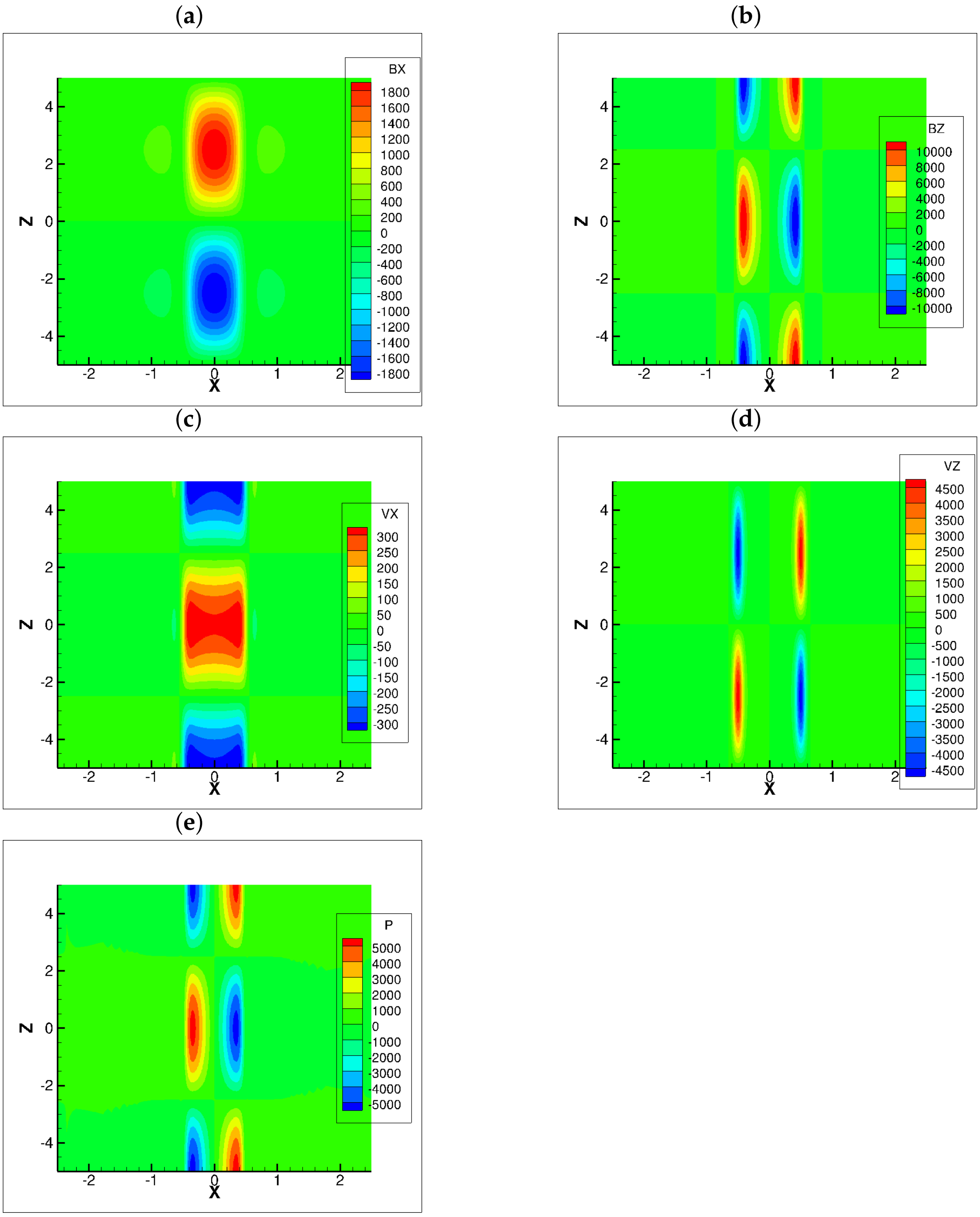

Figure 2. Linear mode structures of (**a**) magnetic field component B_x, (**b**) magnetic field component B_z, (**c**) velocity component v_x, (**d**) velocity component v_z and (**e**) pressure P at $d = 1$.

(**a**)

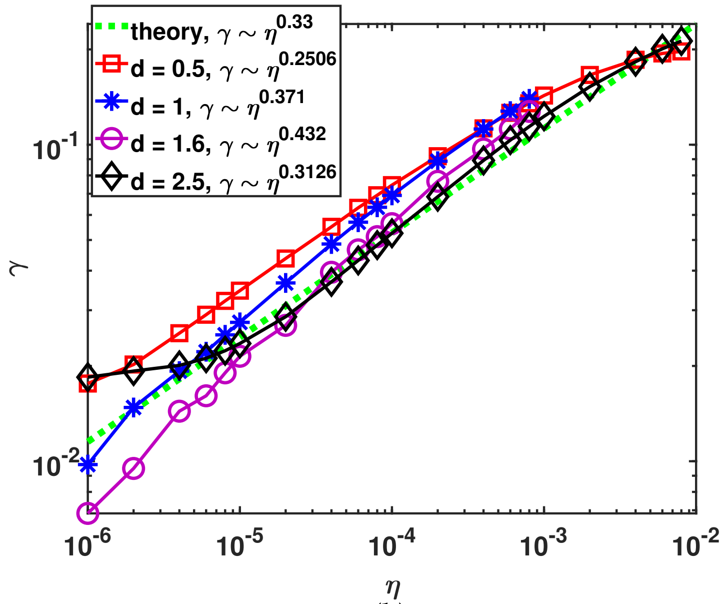

(**b**)

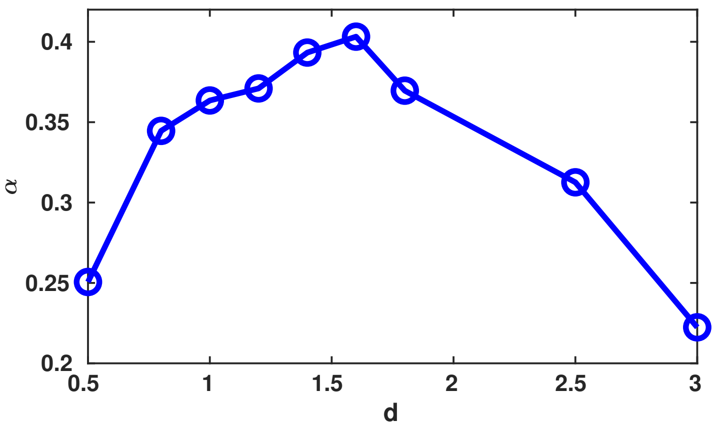

Figure 3. (**a**) Linear growth rates as functions of the resistivity for different distances between the rational surfaces using $\nu \to 0$. (**b**) α (from $\gamma_{lin} = \eta^{\alpha}$) is function of the distances between the rational surfaces.

(**a**)

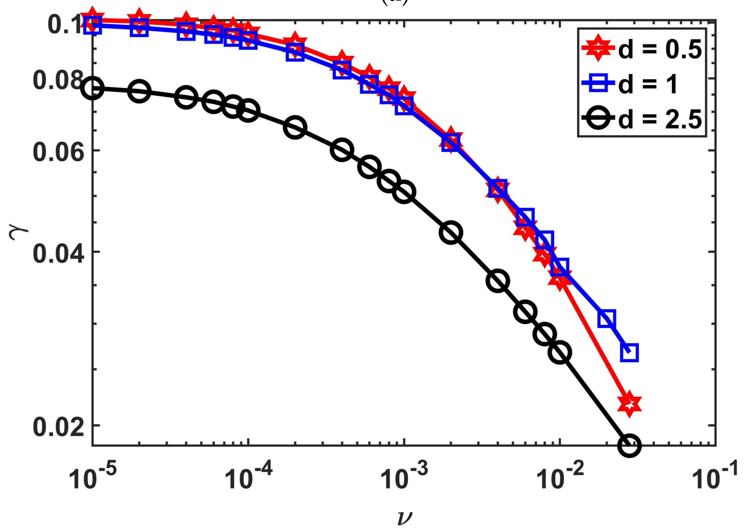

Figure 4. *Cont.*

(**b**)

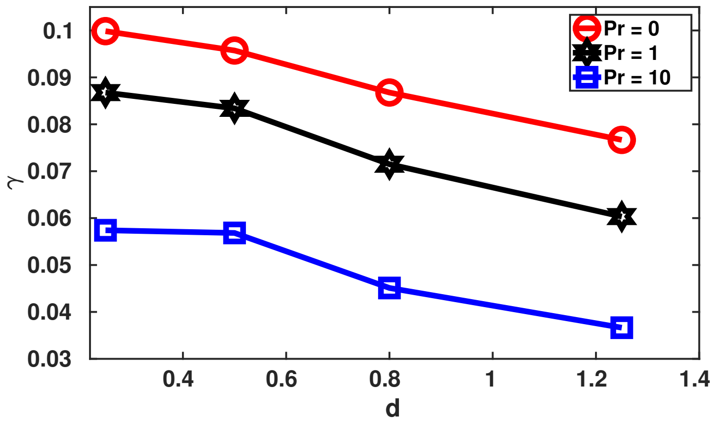

Figure 4. (**a**) Linear growth rates as functions of the viscosity at different distances between the rational surfaces for fixed value of $\eta = 0.00028$. (**b**) Linear growth rates as functions of the distances between the rational surfaces for different Prandtl numbers.

4. Nonlinear DTM and Plasmoids

4.1. Nonlinear DTM Evolution

To study the effects on the nonlinear DTM evolution, one particular case with wave vector $ka = 0.15$ is selected. The viscosity is varied in the form of the Prandtl number in the range $P_r = 0.33, 0.5, 1, 5, 10, 100$ with the fixed resistivity $\eta = 0.00028$ and $d = 1.1$ as the current sheets spacing. A total of 96×96 2D finite elements along a 5th order polynomial basis function in both 2D directions are used in our simulations to ensure numerical convergence (Figure 5).

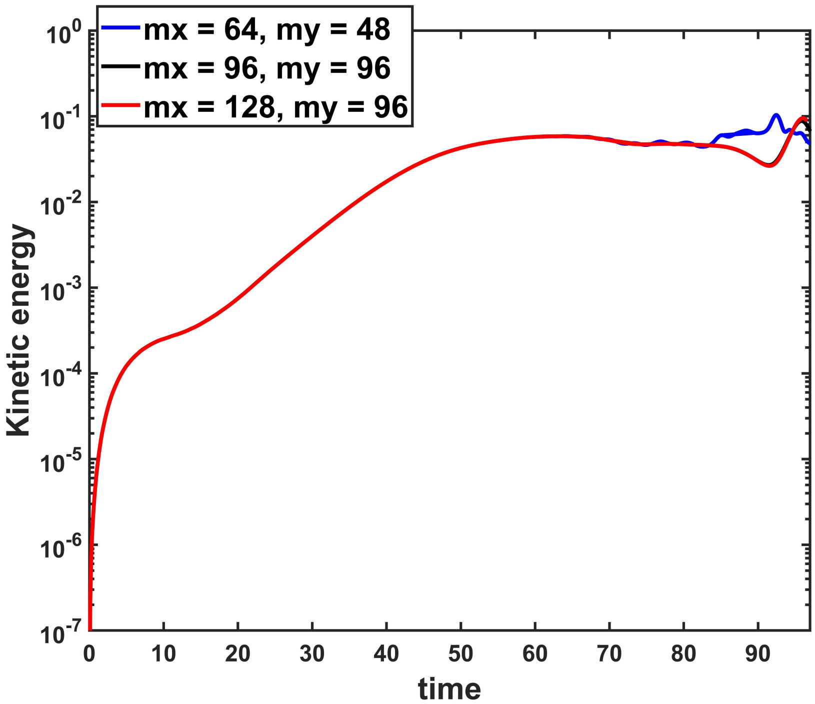

Figure 5. Kinetic energy evolution for different numerical resolutions at $d = 2(x_0) = 1.1$.

Plasma kinetic energy evolution with different values of the Prandtl number are compared in Figure 6, where the black arrows indicate the moments of monster plasmoids generation and the red arrows show the subsequent moments of the normal (small) plasmoid formation. In the case of $P_r = 0.33$, the kinetic energy evolves rapidly during the linear phase and attains the maximum very quickly due to the generation of normal plasmoids, see Figure 6a. By increasing the Prandtl number, such as $P_r = 10$, the kinetic energy evolves through four stages: first is the linear growth evolution stage, second is the slow nonlinear Rutherford phase, third is the fast flux-driven reconnection stage, and the fourth is the decay phase. In our results, by increasing the Prandtl number, the early linear evolution phase and the second phase (Rutherford) evolve for a longer time. Additionally, by increasing $P_r = 100$, the fast flux-driven reconnection phase becomes absent, see Figure 6c.

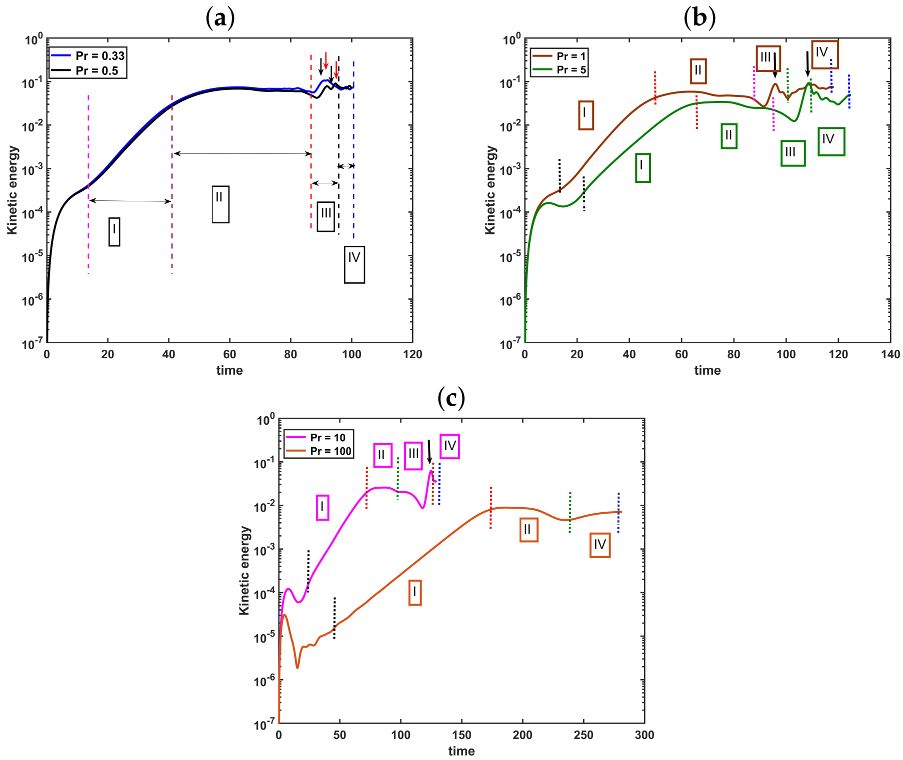

Figure 6. Kinetic energy evolution for (**a**) $P_r = 0.33, 0.5$, (**b**) $P_r = 1, 5$ and (**c**) $P_r = 10, 100$ at $d = 1.1$.

4.2. Plasmoid Formation

The reconnection rate and plasmoids generation in DTMs is different as compared to the STM due to the the different physics between the STM and DTM. A comparison between $P_r = 0.33, 1, 10$ and 100 presents that, due to reconnection, the current sheet becomes much narrower and longer for $P_r = 0.33$, see Figure 7c. After approaching a certain large critical aspect ratio, this current sheet begins tearing, becomes unstable and generates a monster plasmoid in the middle of current sheet which grows in size with the growth of tearing instability, see Figure 7d. With the growth of the monster plasmoid, the secondary current sheets on both sides of the monster plasmoid become more thinner and longer, and will eventually generate two small plasmoids (normal plasmoids), see Figure 7e. Throughout their evolution, as illustrated in Figure 7, all plasmoids within each current sheet merge together, resulting in a significant enlargement of the monster plasmoid, see Figure 7f. As the monster plasmoid grows in size, it moves left and applies force on the primary double tearing mode island. In our results, the primary island makes a curve around the monster plasmoid, see Figure 7f. From this we can conclude that this type of secondary tearing instability can be the reason for the fast increase in kinetic energy from t = 85 to 100 (Figure 6).

However, as we increase the Prandtl number further, the possibility for the production of normal plasmoids decreases quickly because of the wider secondary current sheet. Figures 8 and 9 show the 2D magnetic field lines and 2D contours of current density distribution for the $P_r = 1$ and the $P_r = 10$ cases, respectively. Due to magnetic reconnection, a current sheet forms that surrounds the primary double tearing mode island as an arc, see

Figures 8a and 9a. In these cases we only observe the monster plasmoid, and the production of normal plasmoids was not found in these cases. Figures 8 and 9 show that along with the increase in the size of the plasmoid, it moves towards the left and primary island making an arc-type position around the plasmoid. This current sheet finally disappears and the islands' positions exchange as shown in Figures 7f, 8d and 9d. It is also observed from Figure 10 that for the $\nu = 0.028$, i.e., $P_r = 100$ case there is no monster plasmoid formation (Figure 10). This process shows the dissipation and damping nature of large viscosity. Finally, the reconnection finishes and we obtain the straight field lines after the exhaustion of the initial flux.

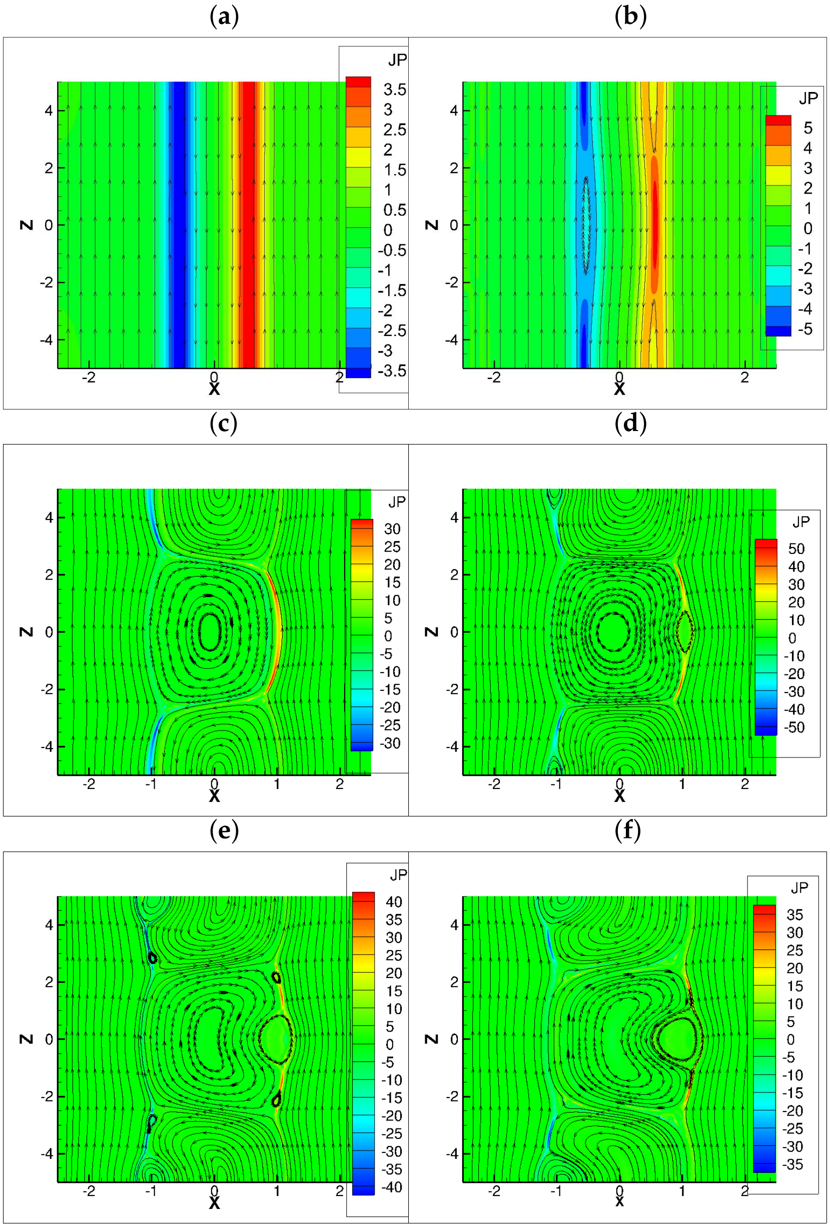

Figure 7. Two-dimensional contours of current density distribution and 2D magnetic field lines with P_r= 0.33 and $d = 1.1$. (**a**) t = 0; (**b**) t = 25; (**c**) t = 85; (**d**) t = 90; (**e**) t = 95; (**f**) t = 100.

Figure 11 shows the evolution of monster plasmoids for different P_r cases and also exhibits the relation among P_r numbers and monster plasmoid width. At lower P_r, with the increase in viscosity, the size of the monster plasmoid grows quickly up to $P_r = 1$. The Prandtl number $P_r = 1$ also divides two regimes for the monster plasmoid width. By increasing the viscosity magnitude in the $P_r < 1$ regime, the plasmoid's width enlarges significantly on the other hand in the $P_r > 1$ regime, it decreases with the rise of viscosity. This behaviour of plasmoid dynamics with viscosity is interestingly matching with the linear and nonlinear reconnection dependence on viscosity in the STM [59].

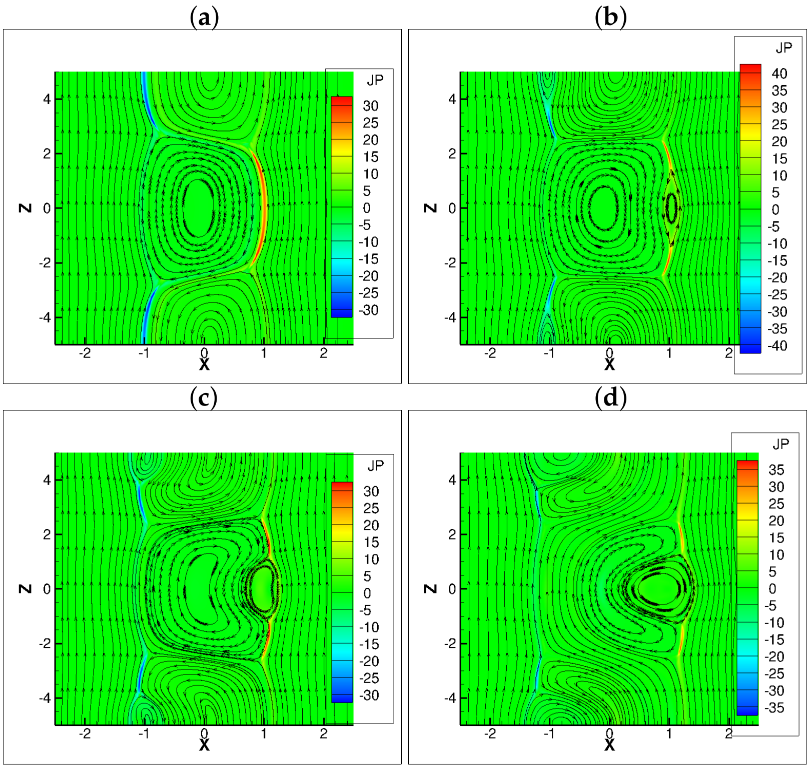

Figure 8. Two-dimensional contours of current density distribution and 2D magnetic field lines with P_r = 1 and $d = 1.1$. (**a**) t = 85; (**b**) t = 95; (**c**) t = 100; (**d**) t = 115.

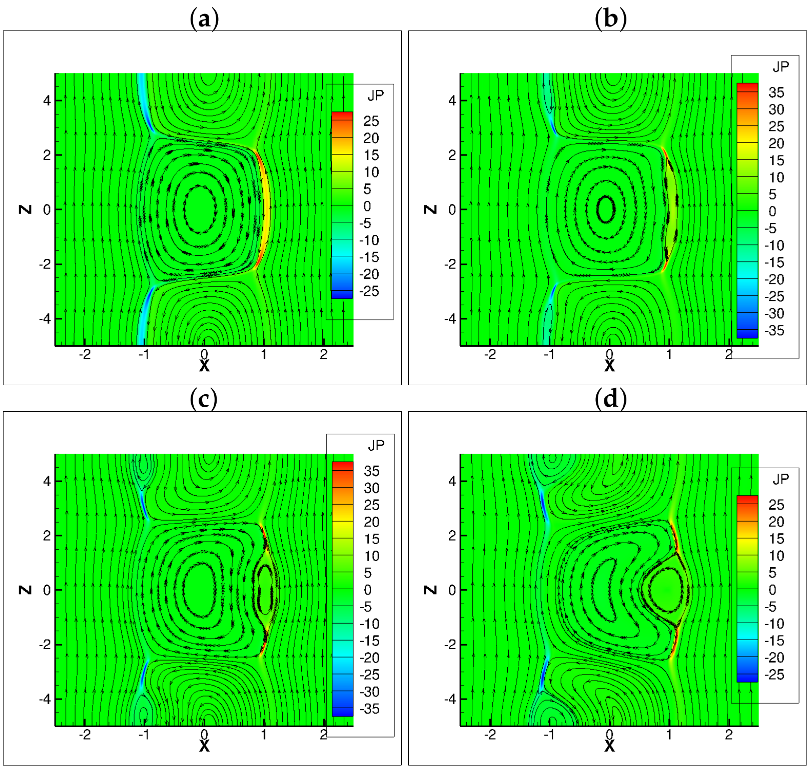

Figure 9. Two-dimensional contours of current density distribution and 2D magnetic field lines with P_r = 10 and $d = 1.1$. (**a**) t = 116; (**b**) t = 120; (**c**) t = 124; (**d**) t = 132.

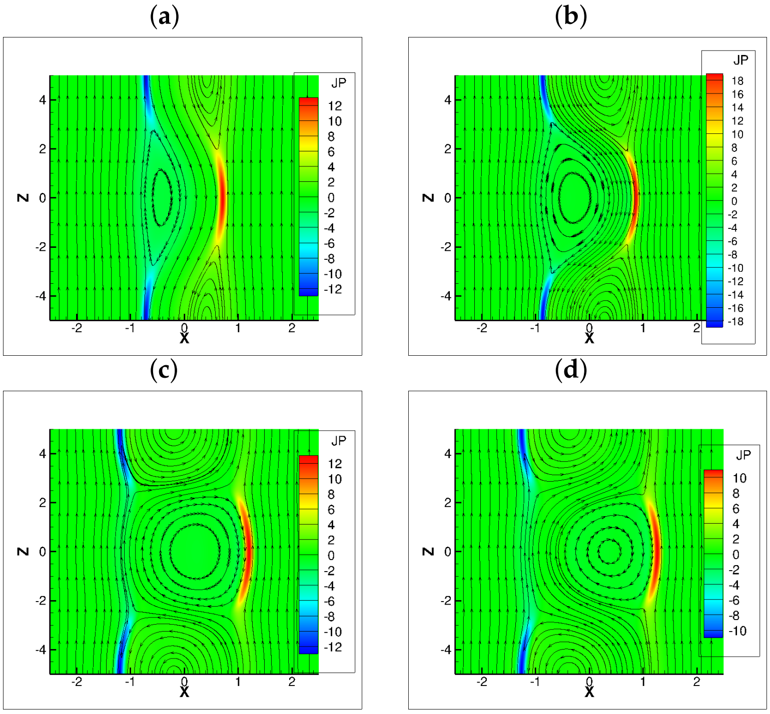

Figure 10. Two-dimensional contours of current density distribution and 2D magnetic field lines with P_r = 100 and $d = 1.1$. (**a**) t = 160; (**b**) t = 185; (**c**) t = 250; (**d**) t = 270.

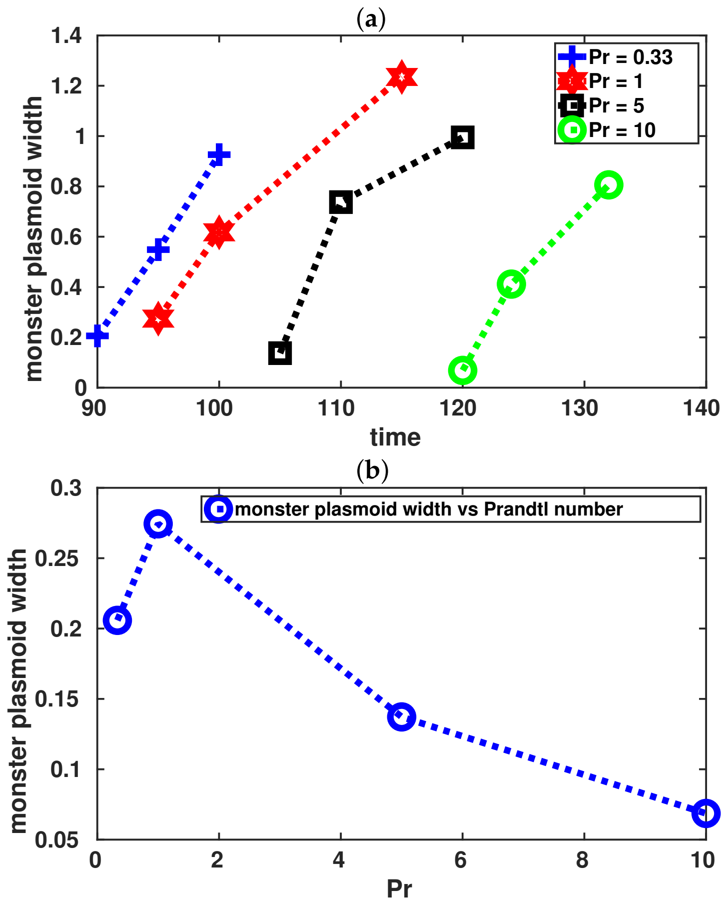

Figure 11. (**a**) Monster plasmoid evolution; (**b**) monster plasmoid width as a function of P_r with $P_r = 0.33, 1, 5$ and 10.

4.3. Flow Pattern and Vortices

The flow pattern and vortex structure developed around the magnetic islands and plasmoids show unique features of the DTM. The viscous effects on the flow pattern associated with the DTM and the corresponding plasmoid formation are also significant (Figures 12–15).

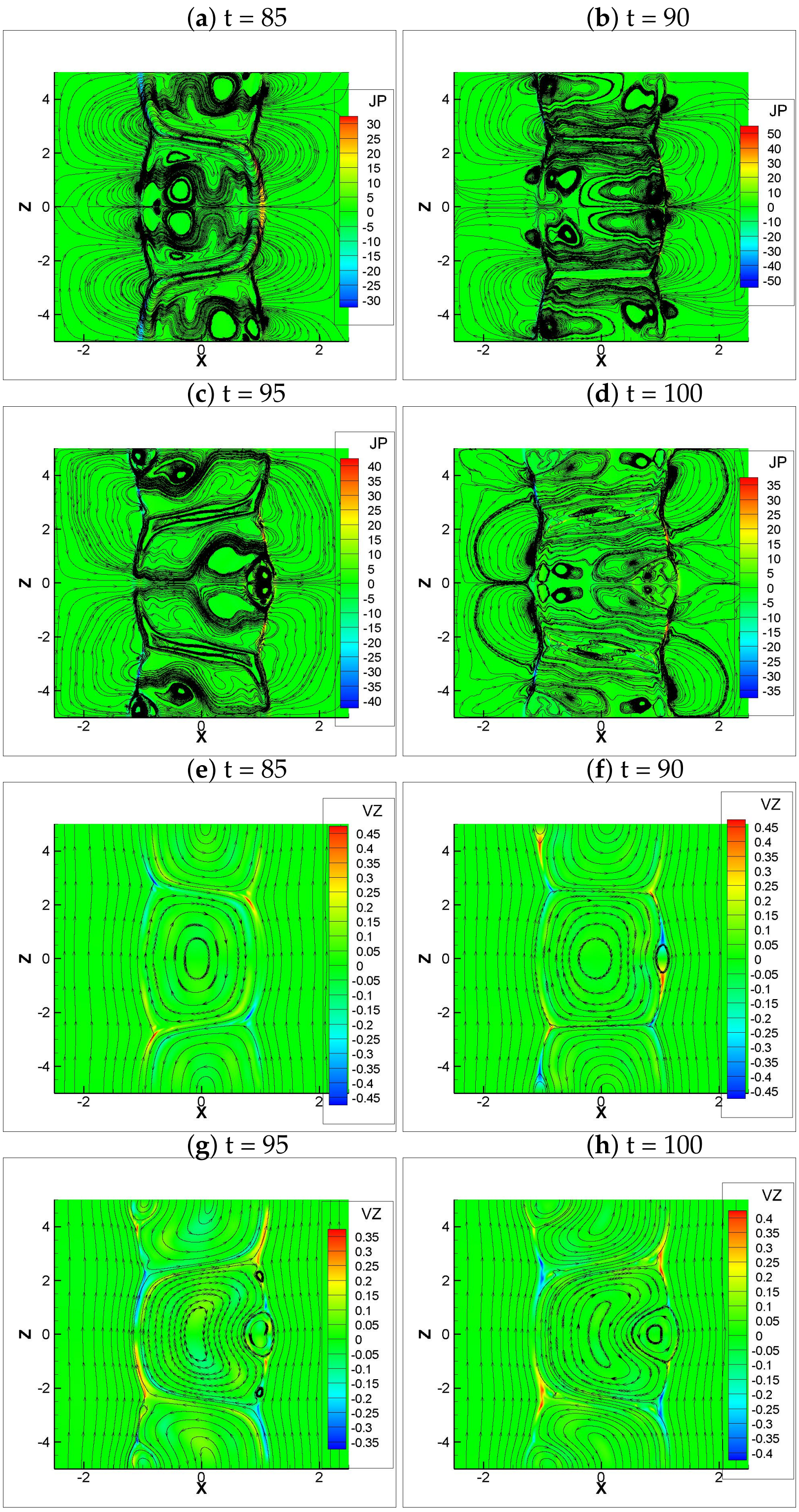

Figure 12. Two-dimensional contours of the current density distribution and flow field stream lines (**a**–**d**), 2D contours of the flow field in the z-direction and 2D magnetic field lines (**e**–**h**), P_r = 0.33 with $d = 1.1$.

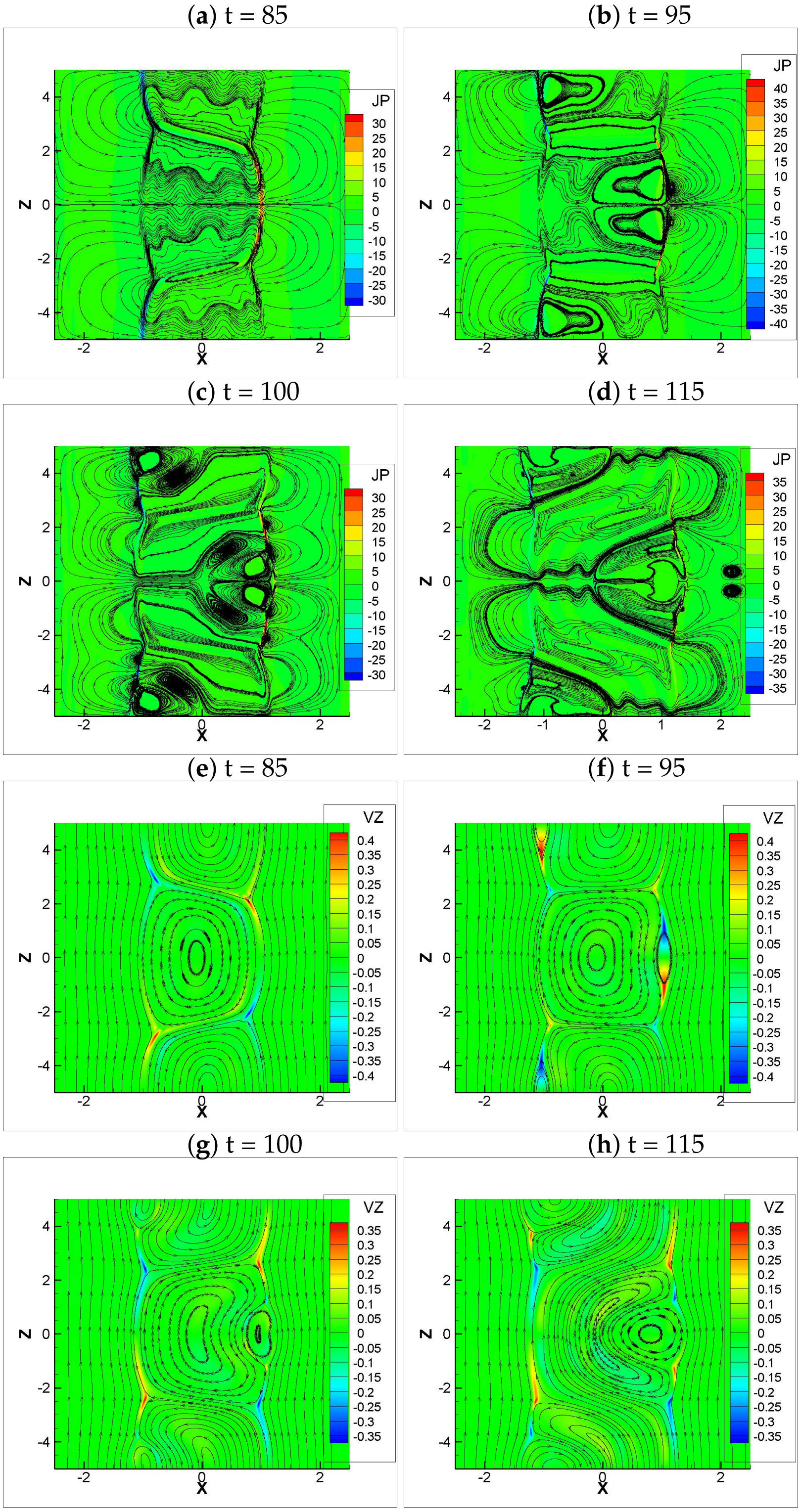

Figure 13. Two-dimensional contours of the current density distribution and flow field stream lines (**a**–**d**), 2D contours of the flow field in the z-direction and 2D magnetic field lines (**e**–**h**), $P_r = 1$ with $d = 1.1$.

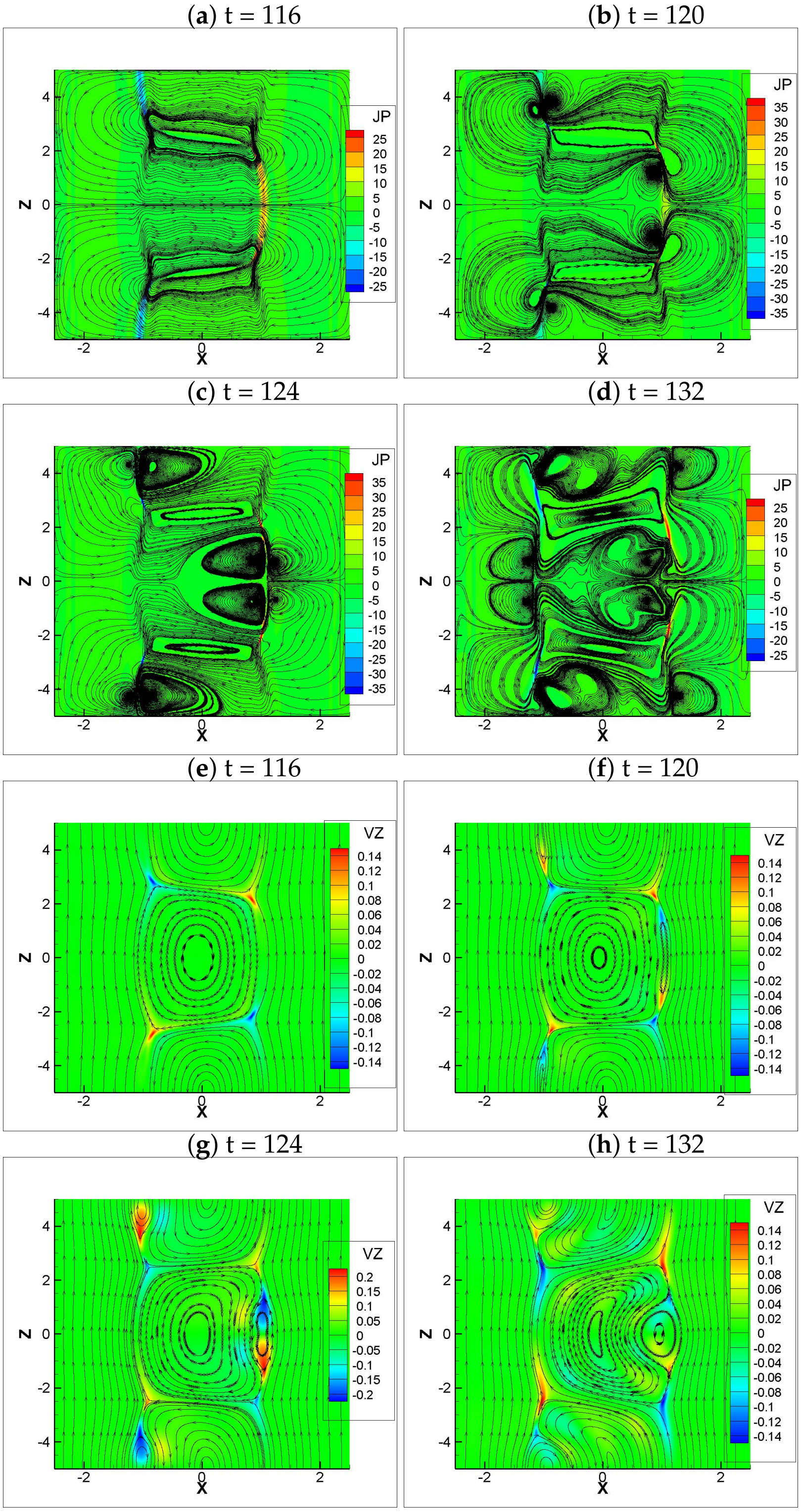

Figure 14. Two-dimensional contours of the current density distribution and flow field stream lines (**a**–**d**), 2D contours of the flow field in the z-direction and 2D magnetic field lines (**e**–**h**), $P_r = 10$ with $d = 1.1$.

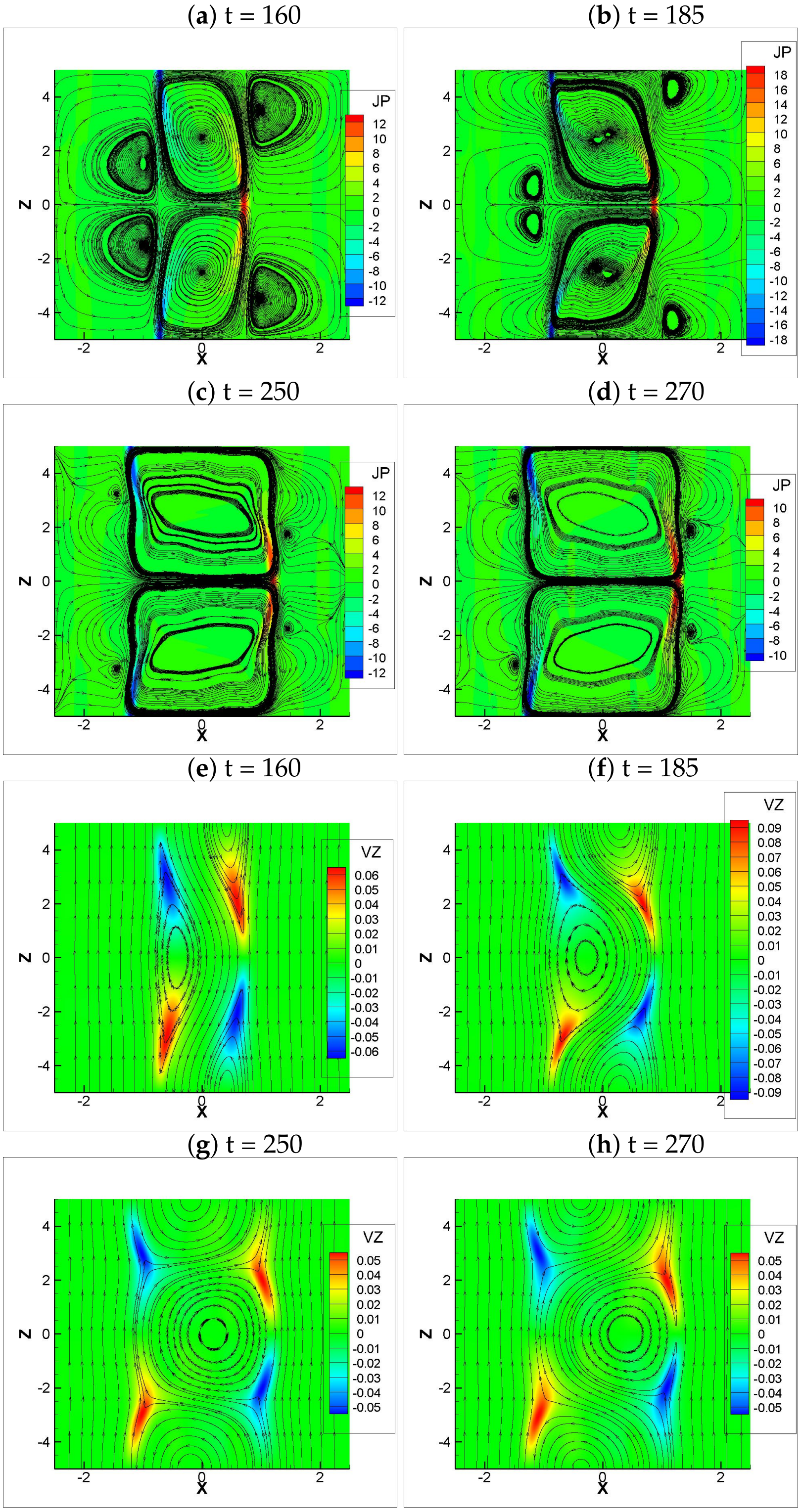

Figure 15. Two-dimensional contours of the current density distribution and flow field stream lines (**a**–**d**), 2D contours of the flow field in the z-direction and 2D magnetic field lines (**e**–**h**),P_r =100 with $d = 1.1$.

In the early stages before the current sheet formation, the size of the magnetic island is so narrow that the plasma flows are restricted within the separated islands. When the width of the island reaches a specific dimension, the plasma converges into the islands, and the currents from both sheets merge, giving rise to the formation of global vortices (Figure 12a). After the collapse of current sheet, thin and intensive shear flow layers form and are localized around the plasmoid on each resonant surface. Observing Figure 12f, it becomes evident that the inner region of the island contains two extreme points at its centers, where a current sheet forms. The outer part of the potential cells flow into the island through the X-point, resulting in a flow through the sheet towards the island around $x = 1.25$. This process causes the expansion of the field lines and intensifies the current sheet, leading to a significant dissipation of magnetic energy. This flow cannot readily leave the island as it is exposed to some kind of force, which produces gradients and the loss of magnetic energy, particularly near the separatrices. As a consequence, at time t = 95 (Figure 12g), we notice that the cells are increasingly concentrated to the island's center. Concurrently, the two sets of cells bearing opposite signs draw nearer, fostering an intensified flow between them caused by the elongation of the two secondary current sheets. Consequently, this leads to the compression of the island. The cells have obviously faded and twisted towards the flow's center at time t = 100 (Figure 12h), whereas the lengths of the two secondary current sheets have increased. The current sheet around the island, however, is no longer concentrated in the outflow zone along the separatrix. Second, opposite sign cells have generated that drive in the opposite direction and make the sheet thin and long. It is also worth noting that the primary cells' exteriors are not entirely destroyed in the area of the sheet. Upon the coupling of magnetic separatrices, thin poloidal shear flow layers and vortex structures still remain long (Figure 12d,h). As we increase the viscosity up to 0.00028 ($P_r = 1$), the vortices formation becomes slower and larger in size. At a larger viscosity, the reconnection and the production of intensive thin poloidal shear flow layers are more inhibited. This fact may contribute as a mechanism to the oscillating decay of kinetic energy at a considerably faster pace when $P_r = 10$ and $P_r = 100$ than when $P_r = 0.33$ and $P_r = 1$ (Figure 6).

5. Summary

In this paper, our focus is on investigating the impact of viscosity on the evolution of DTM-induced plasmoid formation using MHD simulations. We observe that the occurrence of the first peak in the kinetic energy plot aligns with the appearance of the significant plasmoid, referred to as the "monster" plasmoid. When Prandtl numbers (P_r) are small, the production of normal plasmoids causes a sudden increase in kinetic energy at higher levels. Interestingly, we observe a shift occurring at Prandtl number $P_r = 1$, resembling the plasmoid generation pattern seen in the STM case. Adjusting the spacing between the current sheets or modifying the Prandtl number can influence the generation of normal plasmoids, either enhancing or diminishing their production. Additionally, beyond a critical value of the Prandtl number (P_r), the formation of monster plasmoids ceases. The magnetic and flow structures of the DTM, along with the induced formation of plasmoids, differ notably from the STM case. At higher P_r values, the DTM growth becomes slower, and the scales of the magnetic island, the plasmoid, and the flow vortices tend to be larger and more global. Our future research aims to precisely determine the critical P_r value at which the formation of massive plasmoids cease. Additionally, we plan to investigate the influence of two-fluid and 3D effects in our subsequent work.

Author Contributions: N.A.: Writing – original draft, Methodology, Formal analysis. P.Z.: Project administration, review and editing, Visualization, Validation, Funding acquisition. C.S. Validation, Resources, Methodology, Investigation, Supervision. A.A.: review, writing, analysis and editing. S.Z.: code handling and discussion. All authors have read and agreed to the published version of the manuscript.

Funding: This work was financed by National Natural Science Foundation of China (Grants Nos. 42130202 and 51821005), National Key Research and Development Program of China (Grant No. 2022YFA1604600), Fundamental Research Funds for the Central Universities at Huazhong University of Science and Technology (No.2019kfyXJJS193), National Magnetic Confinement Fusion Science Program of China (No. 2019YFE03050004) and the U.S.DOE (Nos. DE-FG02-86ER53218 and DESC0018001).

Institutional Review Board Statement: Not applicable.

Informed Consent Statement: Not applicable.

Data Availability Statement: The supportive data about the results of this paper is accessible from the author upon requisition.

Acknowledgments: We are thankful for the assistance from the NIMROD team. For this research we benefited from the computing system of University of Science and Technology of China. We also thank Haolong Li for his assistance.

Conflicts of Interest: The authors affirm that they do not have any conflicting interests or individual relationships that could have shown to effect the work exhibited in this paper.

References

1. Bierwage, A.; Benkadda, S.; Hamaguchi, S.; Wakatani, M. Fast growing double tearing modes in a tokamak plasma. *Phys. Plasmas* **2005**, *12*, 082504. [CrossRef]
2. Wang, X.-Q.; Wang, X.; Xu, W.-B.; Wang, Z.-X. Interlocking and nonlinear saturation of double tearing modes in differentially rotating plasmas. *Phys. Plasmas* **2011**, *18*, 012102. [CrossRef]
3. Zweibel, E.G.; Yamada, M. Magnetic Reconnection in Astrophysical and Laboratory Plasmas. *Annu. Rev. Astron. Astrophys.* **2009**, *47*, 291. [CrossRef]
4. Akramov, T.; Baty, H. Non-linear growth of double tearing mode: Explosive reconnection, plasmoid formation, and particle acceleration. *Phys. Plasmas* **2017**, *24*, 082116. [CrossRef]
5. Dahlburg, R.; Karpen, J. A triple current sheet model for adjoining coronal helmet streamers. *J. Geophys. Res. Space Phys.* **1995**, *100*, 23489. [CrossRef]
6. Crooker, N.; Siscoe, G.; Shodhan, S.; Webb, D.; Gosling, J.; Smith, E.J. Multiple heliospheric current sheets and coronal streamer belt dynamics. *J. Geophys. Space Phys.* **1993**, *98*, 9371. [CrossRef]
7. Mikic, Z.; Barnes, D.; Schnack, D. Dynamical evolution of a solar coronal magnetic field arcade. *Astrophys. J.* **1988**, *328*, 830. [CrossRef]
8. Yan, M.; Otto, A.; Muzzell, D.; Lee, L. Tearing mode instability in a multiple current sheet system. *J. Geophys. Res. Space Phys.* **1994**, *99*, 8657. [CrossRef]
9. Bowers, K.; Li, H. Spectral energy transfer and dissipation of magnetic energy from fluid to kinetic scales. *Phys. Rev. Lett.* **2007**, *98*, 035002. [CrossRef]
10. Baty, H. Explosive magnetic reconnection in double-current sheet systems: Ideal versus resistive tearing mode. *Astrophys. J.* **2017**, *837*, 74. [CrossRef]
11. Schwartz, S.J.; Kessel, R.L.; Brown, C.C.; Woolliscroft, L.J.; Dunlop, M.W.; Farrugia, C.J.; Hall, D.S. Active current sheets near the earth's bow shock. *J. Geophys. Space Phys.* **1988**, *93*, 11295. [CrossRef]
12. Levinton, F.; Zarnstorff, M.; Batha, S., Bell, M.; Bell, R.; Budny, R., Bush, C.; Chang, Z.; Fredrickson, E.; Janos, A.; et al. Improved confinement with reversed magnetic shear in tftr. *Phys. Rev. Lett.* **1995**, *75*, 4417. [CrossRef] [PubMed]
13. Ishii, Y.; Azumi, M.; Kishimoto, Y. Structure-driven nonlinear instability of double tearing modes and the abrupt growth after long-time-scale evolution. *Phys. Rev.* **2002**, *89*, 205002. [CrossRef] [PubMed]
14. Wang, Z.X.; Wang, X.G.; Dong, J.Q.; Lei, Y.A.; Long, Y.X.; Mou, Z.Z.; Qu, W.X. Fast resistive reconnection regime in the nonlinear evolution of double tearing modes. *Phys. Rev. Lett.* **2007**, *99*, 185004. [CrossRef]
15. Janvier, M.; Kishimoto, Y.; Li, J. Structure-driven nonlinear instability as the origin of the explosive reconnection dynamics in resistive double tearing modes. *Phys. Rev.* **2011**, *107*, 195001. [CrossRef]
16. Priest, E.R. The magnetohydrodynamics of current sheets. *Rep. Prog. Phys.* **1985**, *48*, 955. [CrossRef]
17. Chang, Z.; Park, W.; Fredrickson, E.; Batha, S.; Bell, M.; Bell, R.; Budny, R.; Bush, C.; Janos, A.; Levinton, F.; et al. Off-axis sawteeth and double-tearing reconnection in reversed magnetic shear plasmas in tftr. *Phys. Rev. Lett.* **1996**, *77*, 3553. [CrossRef]
18. Ishii, Y.; Azumi, M.; Kishimoto, Y.; Leboeuf, J. Long timescale plasma dynamics and explosive growth driven by the double tearing mode in reversed shear plasmas. *Nucl. Fusion* **2003**, *43*, 539. [CrossRef]
19. Wang, Z.-X.; Wang, X.; Dong, J.; Kishimoto, Y.; Li, J. Shear flows induced by nonlinear evolution of double tearing modes. *Phys. Plasmas* **2008**, *15*, 082109. [CrossRef]
20. Eriksson, L.-G.; Fourment, C.; Fuchs, V.; Litaudon, X.; Challis, C.D.; Crisanti, F.; Esposito, B.; Garbet, X.; Giroud, C.; Hawkes, N.; et al. Discharges in the JET Tokamak Where the Safety Factor Profile Is Identified as the Critical Factor for Triggering Internal Transport Barriers. *Phys. Rev. Lett.* **2002**, *88*, 145001. [CrossRef]
21. Joffrin, E.; Challis, C.D.; Conway, G.D.; Garbet, X.; Gude, A.; Günter, S.; Hawkes, N.C.; Hender, T.C.; Howell, D.F.; Huysmans, G.T.A.; et al. Internal transport barrier triggering by rational magnetic flux surfaces in tokamaks. *Nucl. Fusion* **2003**, 43, 1167. [CrossRef]
22. Fredrickson, E.; Bell, M.; Budny, R.V.; Synakowski, E. Nonlinear evolution of double tearing modes in tokamaks. *Phys. Plasmas* **2000**, *7*, 4112. [CrossRef]
23. Dong, J.Q.; Mou, Z.Z.; Long, Y.X.; Mahajan, S.M. Study of internal transport barrier triggering mechanism in tokamak plasmas. *Phys. Plasmas* **2004**, *11*, 5673. [CrossRef]

24. Pritchett, P.; Lee, Y.; Drake, J. Linear analysis of the double-tearing mode. *Phys. Fluids* **1980**, *23*, 1368. [CrossRef]
25. de Baar, M.R.; Hogeweij, G.M.D.; Cardozo, N.J.L.; Oomens, A.A.M.; Schüller, F.C. Electron Thermal Transport Barrier and Magnetohydrodynamic Activity Observed in Tokamak Plasmas with Negative Central Shear. *Phys. Rev. Lett.* **1997**, *78*, 4573. [CrossRef]
26. Maget, P.; Huysmans, G.T.A.; Garbet, X.; Ottaviani, M.; Lütjens, H.; Luciani, J.-F. Nonlinear magnetohydrodynamic simulation of Tore Supra hollow current profile discharges. *Phys. Plasmas* **2007**, *14*, 052509. [CrossRef]
27. Ishii, Y.; Azumi, M.; Kurita, G.; Tuda, T. Nonlinear evolution of double tearing modes. *Phys. Plasmas* **2000**, *7*, 4477. [CrossRef]
28. Günter, S.; Yu, Q.; Lackner, K.; Bhattacharjee, A.; Huang, Y.-M. Fast sawtooth reconnection at realistic Lundquist numbers. *Plasma Phys. Control Fusion* **2014**, *57*, 014017. [CrossRef]
29. Zhang, C.; Ma, Z. Nonlinear evolution of double tearing mode with guiding magnetic field. *Phys. Plasmas* **2011**, *18*, 052303. [CrossRef]
30. Nemati, M.; Wei, L.; Wang, Z. Unstable spectra of double tearing modes with antisymmetric shear flow. *Phys. Plasmas* **2018**, *25*, 072119. [CrossRef]
31. Shen, C.; Liu, Z. Magnetic reconnection processes in multiple current-sheet systems with strong flow shear. *Plasma Phys. Control. Fusion* **1998**, *40*, 1. [CrossRef]
32. Shen, C.; Liu, Z.; Zhang, H. Properties of the resistive instability in double current sheet systems with strong shear flows. *Phys. Lett.* **1998**, *249*, 87. [CrossRef]
33. Nemati, M.; Wang, Z.-X.; Wei, L. Formation of plasmoids in multiple current systems. *Astrophys. J.* **2016**, *821*, 128. [CrossRef]
34. Nemati, M.; Wang, Z.-X.; Wei, L. Dynamics of the plasmoid-unstable regime in different multiple-current plasmas. *Astrophys. J.* **2017**, *835*, 191. [CrossRef]
35. Malara, F.; Veltri, P.; Carbone, V. Competition among nonlinear effects in tearing instability saturation. *Phys. Fluids Plasma Phys.* **1992**, *4*, 3070. [CrossRef]
36. Sarto, D.D.; Ottaviani, M. Secondary fast reconnecting instability in the sawtooth crash. *Phys. Plasmas* **2017**, *24*, 012102. [CrossRef]
37. Loureiro, N.F.; Cowley, S.C.; Dorland, W.D.; Haines, M.G.; Schekochihin, A.A. *X*-Point Collapse and Saturation in the Nonlinear Tearing Mode Reconnection. *Phys. Rev. Lett.* **2005**, *95*, 235003. [CrossRef] [PubMed]
38. Nemati, M.; Wang, Z.-X.; Wei, L.; Selim, B.I. Plasmoid instability in double current sheets. *Phys. Plasmas* **2015**, *22*, 012106. [CrossRef]
39. Veranda, M.; Cappello, S.; Bonfiglio, D.; Escande, D.F.; Kryzhanovskyy, A. Magnetic reconnection in three-dimensional quasi-helical pinches. *Rend. Fis. Acc. Lincei* **2020**, *31*, 963. [CrossRef]
40. Loureiro, N.F.; Schekochihin, A.A.; Cowley, S.C. Instability of current sheets and formation of plasmoid chains. *Phys. Plasmas* **2007**, *14*, 100703. [CrossRef]
41. Loureiro, N.F.; Samtaney, R.; Schekochihin, A.A.; Uzdensky, D.A. Magnetic reconnection and stochastic plasmoid chains in high-Lundquist-number plasmas. *Phys. Plasmas* **2012**, *19*, 042303 [CrossRef]
42. Uzdensky, D.A.; Loureiro, N.F.; Schekochihin, A.A. Fast Magnetic Reconnection in the Plasmoid-Dominated Regime. *Phys. Rev. Lett.* **2010**, *105*, 235002. [CrossRef] [PubMed]
43. Huang,Y.-M.; Bhattacharjee, A. Distribution of Plasmoids in High-Lundquist-Number Magnetic Reconnection. *Phys. Rev. Lett.* **2012**, *109*, 265005. [CrossRef] [PubMed]
44. Guo, W.; Ma, J.; Yu, Z. Multiple secondary islands formation in nonlinear evolution of double tearing mode simulations. *Phys. Plasmas* **2017**, *24*, 032115. [CrossRef]
45. Konovalov, S.; Mikhailovskii, A.; Shirokov, M.; Tsypin, V. Transport threshold model of neoclassical tearing modes in the presence of anomalous perpendicular viscosity. *Phys. Plasmas* **2002**, *9*, 4596. [CrossRef]
46. Kaw, P.K.; Valeo, E.; Rutherford, P.H. Tearing modes in a plasma with magnetic braiding. *Phys. Rev. Lett.* **1979**, *43*, 1398. [CrossRef]
47. Ahmad, N.; Ping, Z.; Ahmad, A.; Shiyong, Z. Viscous effects on plasmoid formation from nonlinear resistive tearing growth in a harris sheet. *Plasma Sci. Technol.* **2021**, 24, 015103. [CrossRef]
48. Ali, A.; Li, J.; Kishimoto, Y. On the magnetic reconnection of resistive tearing mode with the dynamic flow effects. *Phys. Plasmas* **2015**, *22*, 042102. [CrossRef]
49. Ali, A.; Zhu, P. Effects of plasmoid formation on sawtooth process in a tokamak. *Phys. Plasmas* **2019**, *26*, 052518. [CrossRef]
50. Aydemir, A. Magnetohydrodynamic modes driven by anomalous electron viscosity and their role in fast sawtooth crashes. *Phys. Fluids Plasma Phys.* **1990**, *2*, 2135. [CrossRef]
51. Dong, J.Q.; Mahajan, S.; Horton, W. Double tearing mode in plasmas with anomalous electron viscosity. *Phys. Plasmas* **2003**, *10*, 3151. [CrossRef]
52. Sovinec, C.; Glasser, A.; Gianakon, T.; Barnes, D.; Nebel, R.; Kruger, S.; Schnack, D.; Plimpton, S.; Tarditi, A.; Chu, M.; et al. Nonlinear magnetohydrodynamics simulation using high order finite elements. *J. Comput. Phys.* **2004**, *195*, 355. [CrossRef]
53. He, Z.; Dong, J.Q.; He, H.; Wang, Z.T.; Long, Y.X.; Mou, Z.Z. Study of nonlinear evolution of tearing modes induced by anomalous electron viscosity. *Phys. Scr.* **2015**, *90*, 125603. [CrossRef]
54. Mao, A.; Wang, Z.; He, X.; Wang, X. Nonlinear evolution and secondary island formation of the double tearing mode in a hybrid simulation. *Plasma Sci. Technol.* **2021**, *23*, 035103. [CrossRef]
55. Takeda, K. Nonlinear viscoresistive dynamics of the m=1 tearing instability. *Phys. Plasmas* **2008**, *15*, 022502. [CrossRef]

56. Wei, L.; Yang, X.; Zheng, S.; Liu, Y. Numerical study of collisionless q = 1 tearing instability in a cylindrical plasma. *J. Plasma Phys.* **2012**, *78*, 663. [CrossRef]
57. Bierwage, A.; Benkadda, S.; Hamaguchi, S.; Wakatani, M. Dynamics of resistive double tearing modes with broad linear spectra. *Phys. Plasmas* **2007**, *14*, 022107. [CrossRef]
58. Ofman, L. Double tearing instability with shear flow. *Phys. Fluids Plasma Phys.* **1992**, *4*, 2751. [CrossRef]
59. Ali, A.; Li, J.; Kishimoto, Y. On the abrupt growth dynamics of nonlinear resistive tearing mode and the viscosity effects. *Phys. Plasmas* **2014**, *21*, 052312. [CrossRef]